ELEMENTA
Science of the Anthropocene

Gao, B, et al. 2021. Study of methane migration in the shallow subsurface from a gas pipe leak. *Elem Sci Anth*, 9: 1. DOI: https://doi.org/10.1525/elementa.2021.00008

RESEARCH ARTICLE

Study of methane migration in the shallow subsurface from a gas pipe leak

Bo Gao[1], Melissa K. Mitton[2], Clay Bell[3], Daniel Zimmerle[3], T. K. K. Chamindu Deepagoda[4], Arsineh Hecobian[5], and Kathleen M. Smits[1,2,*]

With the increased use of natural gas, safety and environmental concerns from underground leaking natural gas pipelines are becoming more widespread. What is not well understood in leakage incidents is how the soil conditions affect gas migration behavior, making it difficult to estimate the gas distribution. To shed light on these concerns, an increased understanding of subsurface methane migration after gas release is required to support efficient leak response and effective use of available technologies. In this study, three field-scale experiments were performed at the Methane Emission Technology Evaluation Center in Colorado State University to investigate the effect of soil textural heterogeneity, soil moisture, and leak rate (0.5 and 0.85 kg/h) on methane migration caused by leaking pipelines. Subsurface methane concentrations, in addition to soil moisture and meteorological data, were collected over time. A previously validated numerical model was modified and used to understand the observed methane distribution behavior. Results of this study illustrate that the influence of soil texture, leak rate, and moisture on subsurface methane distribution is determined by the relative contribution of advection and diffusion and closely related to the distance to the leak source. Advection dominates gas transport within 1–1.5 m of the leak source, driving the migration of high concentration contours. Beyond this distance, diffusion dominates migration of lower concentration contours to the far-field. Although large leak rates initially result in faster and further gas migration, the leak rate has little influence on the diffusion dominated migration farther from the leak source. Soil moisture and texture complicate gas behavior with texture variations and elevated soil moisture conditions playing a dominant role in locally increasing methane concentrations. Scenarios highlight the importance of understanding the effects of soil moisture, texture, and leak rate on gas migration behavior in an attempt to unravel their contribution to the gas concentration within the soil environment.

Keywords: Methane leakage, Gas transport, Pipeline leak, Gas pipe leak, Leak detection and repair, Advection and diffusion

1. Introduction

In the United States, there are over 2.2 million miles of natural gas (NG) distribution mains and service lines (Annual Report Mileage for Gas Distribution Systems, 2020) and subsurface pipeline infrastructure continues to grow to keep pace with the growth in NG usage. Pipelines may leak due to external interference, material failure, earth movement, breakdown of joints, corrosion of unprotected steel, and graphitization of iron pipelines. Pipeline leakage can be catastrophic due to gas buildup, migration in subsurface environments, and ultimately release into the air or into a substructure. Ignition of released gas can have significant impacts on human health, the environment, and the economy (Jackson et al., 2014; U.S. Department of Transportation Pipeline and Hazardous Material Safety Administration, 2020). Methane is a key component of NG, and its subsurface migration and accumulation is especially significant. Although recent technology advances in methane detection have resulted in improved leak detection accuracy and efficiency (e.g., Foster et al., 2019; Ravikumar et al., 2019), efforts are hampered in subsurface pipeline scenarios due to the complex environmental conditions (e.g., soil type, soil disturbance during pipeline laying and boring, neighboring subsurface utilities, ground surface cover), as well as the complexity of gas distribution systems. Therefore,

[1] Department of Civil Engineering, University of Texas, Arlington, TX, USA
[2] Department of Civil and Environmental Engineering, Colorado School of Mines, Golden, CO, USA
[3] Energy Institute and Department of Mechanical Engineering, Colorado State University, Fort Collins, CO, USA
[4] Department of Civil Engineering, University of Peradeniya, Sri Lanka
[5] Department of Atmospheric Science, Colorado State University, Fort Collins, CO, USA

* Corresponding author:
Email: kathleen.smits@uta.edu

a better understanding of how environmental conditions affect methane migration behaviors is key to predicting and mitigating leak incidents.

Advection and diffusion are the two primary mechanisms controlling methane transport in soil, in addition to biological activity (e.g., microbial oxidation). However, their contribution to methane migration process varies based upon subsurface properties, as well as atmospheric conditions. For example, soil textural heterogeneities due to the existence of low permeable layers (e.g., clay layers) in sandy soil will result in methane distribution patterns that differ from those in a homogeneous system. Faster gas flow in higher permeability sand provides a preferential pathway for advective methane transport, while clay has a larger diffusivity than sand and therefore increases diffusion-controlled migration. Besides, soil moisture influences methane migration in unsaturated soils due to changes in methane solubility, oxidation, tortuosity, and gas-filled porosity. An increase in soil moisture will reduce the gas permeability, thereby decreasing methane advection. The increased soil moisture will also increase tortuosity for gas flow and thus decrease methane diffusivity. However, the reduced methane transport may cause local methane accumulation and increase advection in those areas. This may result in reverse influences on methane distribution. Moreover, there are many other factors influencing subsurface methane migration behaviors (e.g., Keskikuru et al., 2001; Poulsen et al., 2003; Patterson and Davis, 2009; Bahlmann et al., 2020), such as pipeline pressure, gas composition when pipelines carry heavier (C^{2+}) hydrocarbons, construction at/below ground, and soil–atmosphere interactions. Despite these uncertainties, only a limited number of studies combine experimental and numerical approaches to investigate subsurface methane migration under different environmental conditions.

Most of the previous experimental studies investigating the migration of methane or other gases in soil or porous media were conducted at the laboratory scale using either a one-dimensional uniformly packed soil column (e.g., Karl-Heinz et al., 2004; Hibi et al., 2009, 2012; Levintal et al., 2017; Pourbakhtiar et al., 2017) or a soil tank (e.g., Deepagoda et al., 2016; Poulsen et al., 2017, 2018, Van De Ven et al., 2020). These studies are limited by their scales and experimental materials (e.g., silica sand), thus cannot be directly applied to the investigation of migration in natural soil. A few field-scale studies have demonstrated that methane migration length can vary from 2 to 10 m (Okamoto and Gomi, 2011; Xie et al., 2015; Yan et al., 2015) as it leaks from distribution pipelines. Analyses of catastrophic leak incidents indicate that the gas may migrate distances of 30 m or more within 15 min of a large pipeline leak incident (Heldenbrand and Saavedra, 2019). These results demonstrate the importance of conducting realistic field-scale studies (e.g., Iwata et al., 1992; Okamoto and Gomi, 2011; Xie et al., 2015; Yan et al., 2015). Ulrich et al. (2019) performed a study to understand subsurface methane leaks through aboveground methane detection methods, demonstrating the importance of considering the effects of subsurface processes with respect to aboveground methane concentrations. Additionally, commonly utilized aboveground detection methods do not translate directly to underground methane leaks due to significant differences in (a) the diffuse presentation of subsurface leaks compared to point sources from above ground equipment leaks, (b) the environmental conditions near and below ground, and (c) the extended geometry of pipeline systems. Improving the effectiveness of aboveground detection methods applied to pipeline emission scenarios requires a better understanding of the subsurface methane migration behavior.

Although previous laboratory- and field-scale studies provide some insight into such migration behaviors, to date, no study has systematically investigated field-scale methane migration behavior due to the effects of leak rate, soil texture, and soil moisture, as well as the corresponding underlying mechanisms. For numerical approaches, most of the previous studies, which consider methane (or other gases) moving in variably saturated soil or diffusing in a multiple-component gas mixture, did not include the influence of atmospheric wind speed on gas transport from the subsurface into the atmosphere (e.g., Hibi et al., 2009; Okamoto and Gomi, 2011; Yao et al., 2017; Wang et al., 2019; Taherdangkoo et al., 2020; Wang et al., 2020). The authors found limited studies to incorporate atmospheric effects (Oldenburg and Unger, 2004; Basirat et al., 2015), all of which require co-simulation in the atmospheric domain that greatly increases computational cost.

Therefore, this study aims to investigate methane migration in variably saturated soil under varying subsurface conditions to provide new insights into the migration mechanisms through controlled field-scale experiments, as well as modeling for auxiliary understanding. The key hypotheses of this study are (1) the subsurface migration of multicomponent gas mixtures is predominately controlled by the subsurface soil heterogeneity, moisture conditions, leak rate, and to a lesser degree, the near surface atmospheric conditions (i.e., wind, pressure, and temperature) and (2) the degree to which the above controlling parameters affect the transport behavior can be evaluated using a controlled field-scale experimental test system linked with numerical modeling.

2. Materials and methods

2.1. Methane Emission Technology Evaluation Center (METEC) field test bed description

A series of controlled field-scale experiments were conducted at the METEC, Colorado State University, Fort Collins, CO, USA. METEC houses a unique underground pipeline test bed that allows for the simulation of underground pipeline leaks at known leakage rates in varying subsurface (e.g., soil type, texture, moisture, leak depth, and leak direction) and surface (e.g., precipitation, temperature, wind speed, surface obstruction, and vegetation) conditions, allowing for both control and measurement of subsurface and surface conditions on a continuous basis. **Figure 1** shows the schematic of the test bed, which consists of a homogeneous sand bed adjacent to a layered sand bed. Each bed is 5 m long, 5 m wide, and 2 m in depth below ground surface (BGS). Inside the layered sand bed, three clay lenses, which are 0.6 m long horizontally,

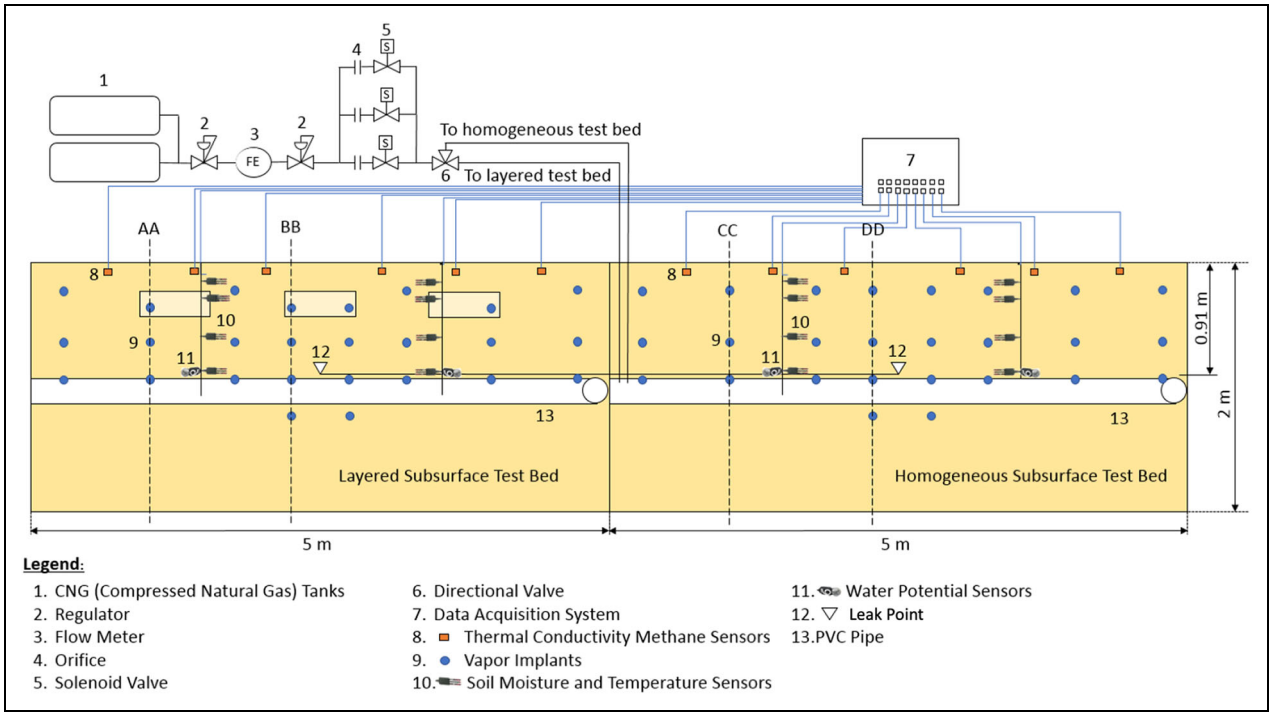

Figure 1. Schematic of the Methane Emission Technology Evaluation Center test bed profile. The lighter colored boxes in the layered test bed represent the locations of the three clay layers. DOI: https://doi.org/10.1525/elementa.2021.00008.f1

3 m long laterally, and 0.2 m thick, are located side by side at a depth of 0.25 m (top of clay lens to the ground surface) BGS. The middle clay layer is centered just above the leak point of the layered test bed and the two adjacent clay layers are 0.61 m apart (**Figure 2**). The dimensions of the clay layers were selected to simulate noncontinuous heterogeneities that also scaled with the limited size of the test bed. A schedule 40 polyvinyl chloride (PVC) pipe is located at 0.91 m BGS, representing a leaking pipeline. The depth was selected based on the natural soil cover requirements for buried pipelines which ranges from 24 to 48 inches, depending on the type, class, and location of the pipeline (Electronic Code of Federal Regulations §192.327 Cover, 2021). Here, the size and depth of burial for the pipelines were selected to be representative of NG distribution mains. Stainless-steel tubing running adjacent to this PVC pipe transports the distribution grade NG to the predetermined leak points at the horizontal middle of each sand bed. The gas was emitted from the tubing to the surrounding unsaturated zone through a vent screen to prevent clogging. Compressed NG with 85%vol–95%vol methane was provided from two 145-L cylinders with predesigned flow rate (**Table 1**). The flow rate from the cylinders was controlled using pressure regulation and solenoid valves in series with precision orifices.

2.2. Test bed construction and measurement

The test beds were dry packed by hand to ensure uniform packing to represent a homogeneous system. The clay layers were accomplished by packing three 3 m × 0.61 m × 0.2 m wooden forms with clay to the desired porosity. The forms were then removed before packing the overlying sand layer. Sensors and vapor implants were installed during packing to avoid site disturbance. Partially saturated conditions of the test beds were achieved by wetting the soil surface with a sprinkler system for approximately 8 h before the start of experiments. Properties of the sand and clay in the test beds were obtained through laboratory tests, as shown in **Table 2**. Microbial methane oxidation was assumed negligible due to the short duration (8 h) of individual experiments and the presence of only trace amounts of organic carbon in the sand and clay (approximately 0.5%).

Vapor implants (Model 213860, Geoprobe, Salina, KS) were installed in the test beds as the main mode of soil gas sample collection. They were attached to 6.35-mm outside diameter polyethylene tubing (Model 601062, Geoprobe, Salina, KS) that lead to the soil surface. At the soil surface, the tubing was finished with a self-sealing silicone tubing adapter (Model 213746, Geoprobe, Salina, KS) and a polyethylene valve. A total of 75 implants were installed in each of the homogenous and layered beds at depths of 0.2, 0.61, 0.91, and 1.2 m BGS (see **Figure 1**). **Figure 2** shows the sampling locations from the top view of the test beds. Along the *x* direction, implants were arranged in two transects: II in the homogeneous bed and GG in the layered bed. Along the *y* direction, implants were arranged in two transects: EE in the homogeneous bed and FF in the layered bed.

Vapor implant sampling was conducted in accordance with ASTM D7648-12. This sampling method requires flowrates under 200 mL per minute and pressures under 100 inches of water. These conditions did not allow for the accumulation of water in the sampling tubes under the

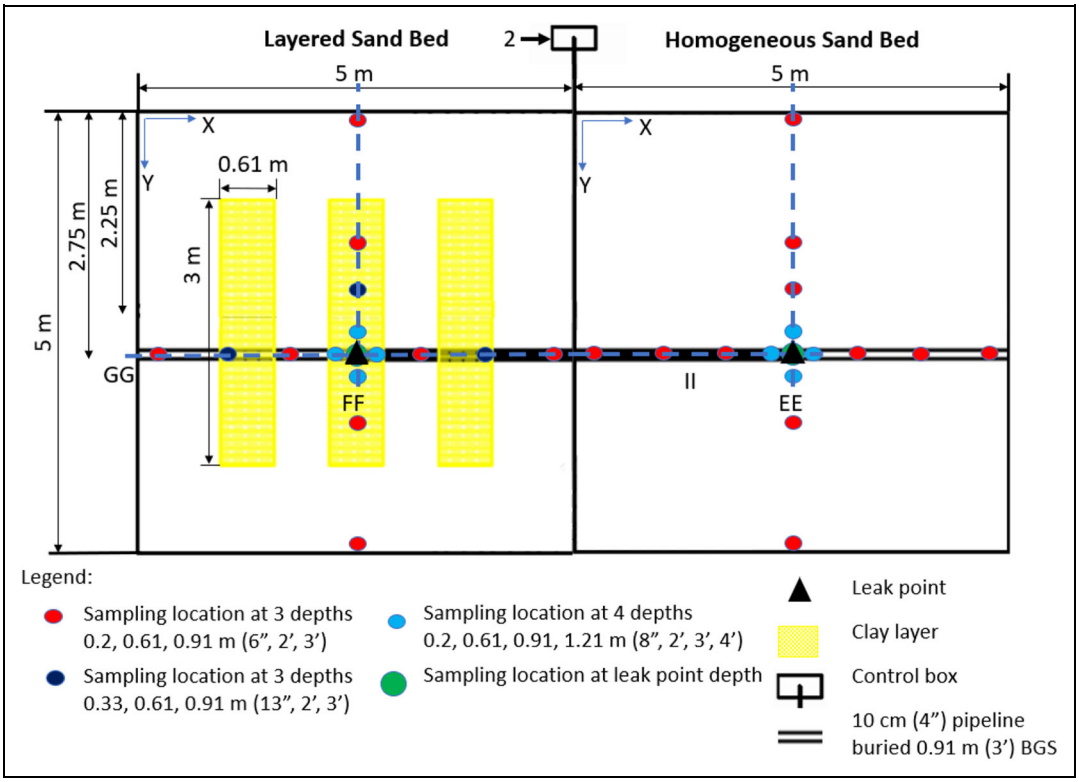

Figure 2. Plan view of homogeneous and layered test beds. The colored circle symbols represent the manual sampling locations. DOI: https://doi.org/10.1525/elementa.2021.00008.f2

Table 1. Experimental cases and description. DOI: https://doi.org/10.1525/elementa.2021.00008.t1

Case #	Textural Configuration	Leak Rate kg/h (Liters per Minute)	Average Wind Speed m/s	Average Saturation
1	Homogeneous	0.5 (13)	1.2	0.14
2	Homogeneous	0.85 (22)	1.3	0.14
3	Layered soil	0.81 (21)	1.6	Sand 0.15, Clay 0.38

Table 2. Physical properties of the sand and clay in the test beds. DOI: https://doi.org/10.1525/elementa.2021.00008.t2

Soil Type	Porosity	Permeability (m^2)	van Genuchten Parameters		
			S_{wr}	α (m^{-1})	n
Sand	0.35	2.90E-11	0.034	15.8	3.58
Clay	0.48	3.82E-14	0.053	6.7	4.17

dry or partially saturated conditions. Samples from the collection vials (0.1 mL) were analyzed for methane with gas chromatography–mass spectrometry (HP 6980 Series GC) using a high split 150:1 injection method at a flowrate of 1.2 mL/min. The analysis occurred under isothermal conditions, at 38 °C, with helium as the carrier gas. Duplicates and blanks were analyzed regularly to ensure accurate and repeatable results. The average standard deviation of all duplicated samples was 1.93%vol methane.

In addition to the manual gas samples and analysis, the methane concentrations near the soil surface were obtained using thermal conductivity methane sensors (New Cosmos Electric CO, Osaka, Japan). According to the manufacturer and subsequently tested in the lab, the sensors measure methane from 0% to 100% volume with a resolution of 0.5%volume under temperatures −10 °C to +40 °C and 10%–85% relative humidity. Six sensors were buried 7.6 cm BGS in the homogeneous and layered test beds, spaced evenly across the horizontal cross section (see **Figure 1**). Data were collected every minute using a CR1000 data logger (Campbell Scientific, Inc. Logan, UT).

In addition to methane measurements, a network of precalibrated sensors (5TM, METER Group, Pullman, WA) was installed within the test beds to monitor soil moisture and temperature. The sensors were connected to an AM16/38b multiplexer (Campbell Scientific, Inc. Logan, UT) and CR1000 data logger (Campbell Scientific, Inc. Logan, UT) for data storage. At 6 m aboveground surface, an Ultrasonic Anemometer (Model 81000, RM Young, Traverse City, Michigan) was installed to measure the average wind speed.

2.3. Experimental methods

Three experiments were completed for this study considering two soil textural configurations (homogeneous and layered) and two leak rates (0.5 and 0.85 kg/h), as shown

in **Table 1**. The first leak rate was selected to represent large NG leaks during walking surveys (von Fischer et al., 2017). The second leak rate was originally selected as double the first, but due to some equipment limitations, the observed leak rate was 0.85 kg/h. Each experiment was started by regulating the gas pressure and opening the solenoid valve to achieve the desired leak rate. Soil moisture and temperature were measured every minute at the predesigned locations (**Figure 1**). Gas concentration within the soil profile was sampled every hour. The thermal conductivity methane sensors, at 7.6 cm BGS, collected concentration data every minute. Due to safety constraints, each experiment ran for a total of 8 h.

2.4. Numerical model

In addition to the field experiments, numerical modeling was used as an auxiliary approach to assist understanding the phenomena and mechanisms of methane transport through the shallow soil environment. The model was developed on the basis of Deepagoda et al. (2016), which was validated by their laboratory experiments, and on the basis of Cho et al. (2020), which was specifically validated for the METEC site. The most significant difference between the model in this study and Deepagoda et al. (2016) is that the influence of near-surface wind speed on gas flux from soil is included in the model presented here.

The modified model assumes two-phase (liquid water and gas) flow and two-component (methane and air) transport in unsaturated soil under isothermal conditions. The dissolution of methane in soil water is neglected due to its low solubility in water (0.022 mg/mL) and low water saturation within the shallow subsurface. Under these assumptions, the fluid flow in the unsaturated soil can be described based on mass balance:

$$\phi \frac{\partial(\rho_i S_i)}{\partial t} + \nabla \cdot (\rho_i \mathbf{u}_i) = 0, \quad (1)$$

where the subscript i (= w, g) represents the liquid water (w) and gas (g) phase, ϕ is the porosity, ρ_i (kg/m^3) and S_i are the density and saturation of i phase, respectively, and $\mathbf{u}_i$ (m/s) is the velocity of i-phase, which is described based on Darcy's law:

$$\mathbf{u}_i = -\frac{\mathbf{K}_{\text{int}} k_{ri}}{\mu_i}(\nabla p_i + \rho_i \mathbf{g}), \quad (2)$$

where $\mathbf{K}_{\text{int}}$ (m^2) is the intrinsic permeability of soil, k_{ri} is the relative permeability of i-phase, and μ_i (Pa·s) and p_i (Pa) are the viscosity and pressure of i-phase, respectively. The van Genuchten (1980) model (van Genuchten, 1980) is used to determine the relationship between saturation and capillary pressure, as well as the relative permeability.

The transport of the methane component in the gas phase is described by:

$$\phi \frac{\partial\left(\rho_g w_m S_g\right)}{\partial t} + \nabla \cdot \left(\rho_g w_m \mathbf{u}_g\right) - \nabla \cdot \left[\mathbf{D}_m \nabla\left(\rho_g w_m\right)\right] = 0, \quad (3)$$

where w_{m} is the mass fraction of methane (m) in the gas phase; $\mathbf{D}_m$ (m^2/s) is the effective diffusion coefficient tensor in the unsaturated zone determined by Millington and Quirk's (1961) model.

Due to the assumption of a homogeneous system, the numerical simulations were completed using a 2-D Cartesian vertical computational domain (40 m × 5 m) representing the unsaturated zone. The leak point was set at the horizontal middle ($x = 0$) of the domain and 0.91 m below the top surface. The domain bottom was treated as a symmetric boundary. Hydrostatic water pressure determined by the saturation at ground surface and bottom was assigned at the left and right sides of the domain. At the top surface, an atmospheric pressure was assumed. A flux top boundary condition (Brutsaert, 1982; Vanderborght et al., 2017) was used to incorporate the effect of atmospheric wind speed for methane transport from the soil into the free air:

$$\mathbf{n} \cdot \left[\rho_g w_m \mathbf{u}_g - \mathbf{D}_m \nabla\left(\rho_g w_m\right)\right] = \lambda \rho_g \left(w_{m,s} - w_{m,a}\right), \quad (4)$$

where $w_{\text{m, s}}$ and $w_{\text{m, a}}$ are the mass fraction of methane at soil surface and the reference plane in the atmosphere where the wind speed is measured, respectively. In this study, $w_{\text{m, a}}$ is assumed as zero based on the wind speed measurement location 6 m above ground; λ (m/s) is the mass transfer coefficient determined by (Camillo and Gurney, 1986):

$$\lambda = \frac{\kappa u_{\text{ref}}}{\left[\ln\left(\frac{z_{\text{ref}} - d_0}{z_{0m}}\right)\right]^2}, \quad (5)$$

where κ (=0.41) is the von Kármán constant, u_{ref} (m/s) is the wind speed measured at the reference plane z_{ref} (m) above ground, d_0 (m) (=0 for a flat surface) is the displacement height, and z_{0m} (m) is the momentum roughness length and assumed as 0.03 m (Wieringa, 1980) in this study.

3. Results and discussion

In this section, we first show the observed subsurface methane migration behavior (other NG components are not included), followed by a more detailed discussion using the experimental data and modeling. All methane concentration plots in this section were developed using the mapping software program Surfer (Golden Software, Golden, CO) and the point kriging interpolation method.

3.1. General subsurface methane migration behavior

Figure 3 shows the distribution of the observed methane concentration for Case #2 at three different times along two different transects: II (parallel to the pipeline) and EE (perpendicular to the pipeline). These plots only show half of the total cross section as symmetric distribution to the leak point ($x = 0$) is assumed for each transect due to homogeneous packing. The trends in all the plots are similar, showing relatively concentric concentration contours centered on the leak point. The slight variations between the two transects presented here (II and EE) are

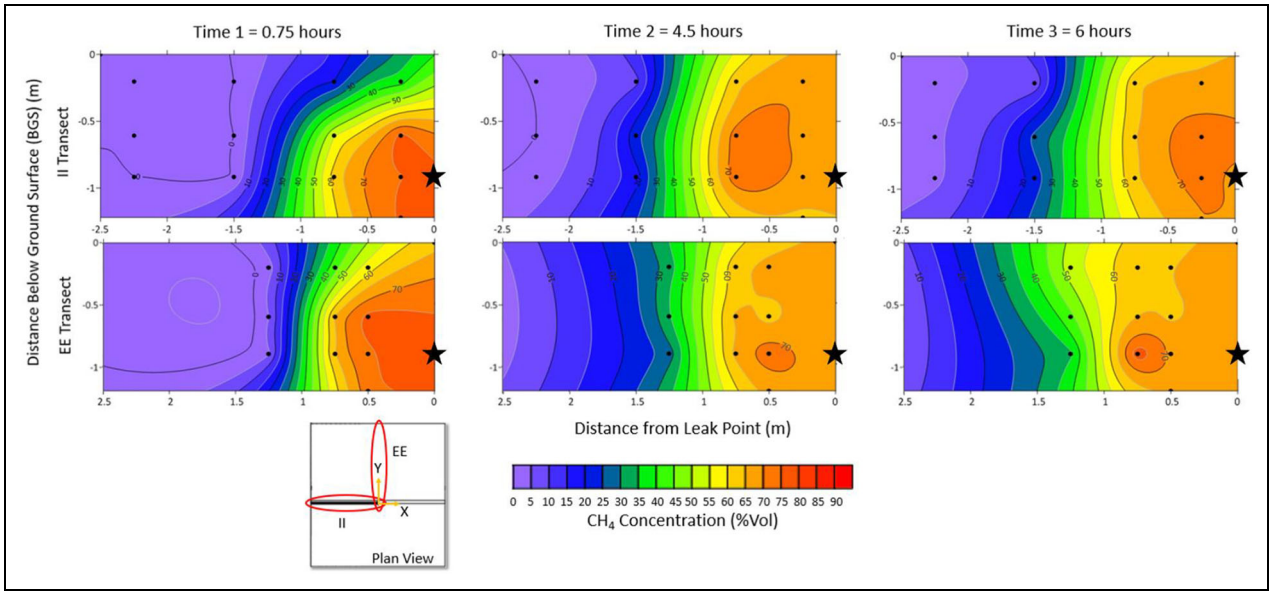

Figure 3. Observed methane concentration plots for Case #2 along the II and EE transect. The leak point is located at (0, –0.91; demarcated by the black star icon). DOI: https://doi.org/10.1525/elementa.2021.00008.f3

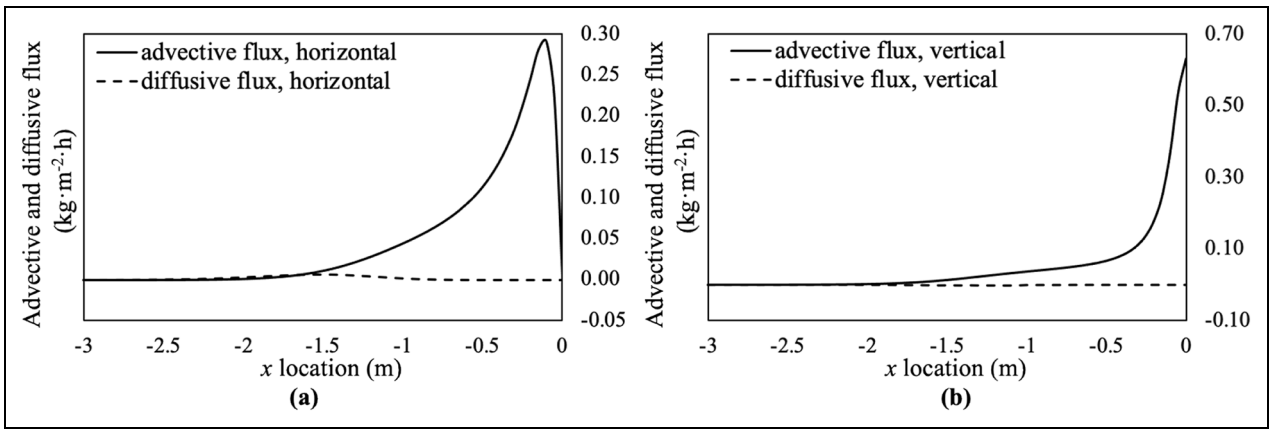

Figure 4. Comparison of simulated advective and diffusive fluxes at $t = 6$ h along a horizontal line 0.8 m below ground surface. (a) Horizontal component value. (b) Vertical component value; note difference in vertical scale. Figures show half of the total cross section with the leak point located at $x = 0$. DOI: https://doi.org/10.1525/elementa.2021.00008.f4

most likely due to unavoidable, small differences in porosity incurred during the sand bed packing, resulting in localized anisotropy. In the horizontal or lateral direction, the contours are almost symmetric. A larger concentration gradient is observed in the area farther from the leak point, represented by dense contours. Approaching the leak point, the high concentration contours are distributed more sparsely. In the vertical direction, the contours display an upward-bulging shape, denoting that methane preferentially moves upward.

The horizontal and vertical migration behaviors of methane occur because the advection, caused by gas release, plays a dominant role near the leak source. **Figure 4** illustrates the comparison between the simulated advective and diffusive flux along a selected transect located 0.8 m below the top surface of the computation domain. At the area close to the leak point, advective flux is much larger than the diffusive flux, especially in the vertical direction (**Figure 4b**), which determines the upward-bulging shape of the concentration contour. Farther from the leak point (e.g., 1.5 m away), the advection effect caused by gas release gradually attenuates to a minimum value, and its dominance disappears.

Additionally, as seen in **Figure 3**, the methane concentration shows a distinct distribution behavior closer to the start of the initial leak compared to later times. Specifically, at early times (e.g., 0.75 h), there is a pronounced expansion of high concentration contours close to the leak point, whereas at later times (e.g., from 4.5 h to 6 h), the expansion of these high concentration contours slows and is less obvious. In contrast, lower concentration contours located farther from the leak point continue to expand several hours after the leak start. Although the expansion is not as apparent as the early expansion of high

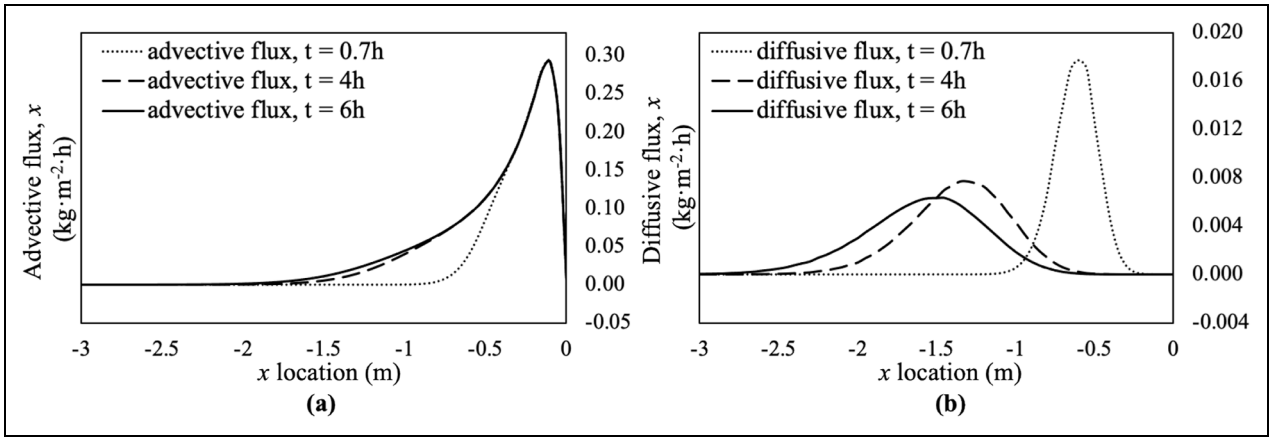

Figure 5. Simulated horizontal component value of the (a) advective and (b) diffusive fluxes along a horizontal line at 0.8 m below ground surface at $t = 0.7$, 4, and 6 h; note difference in vertical scale. DOI: https://doi.org/10.1525/elementa.2021.00008.f5

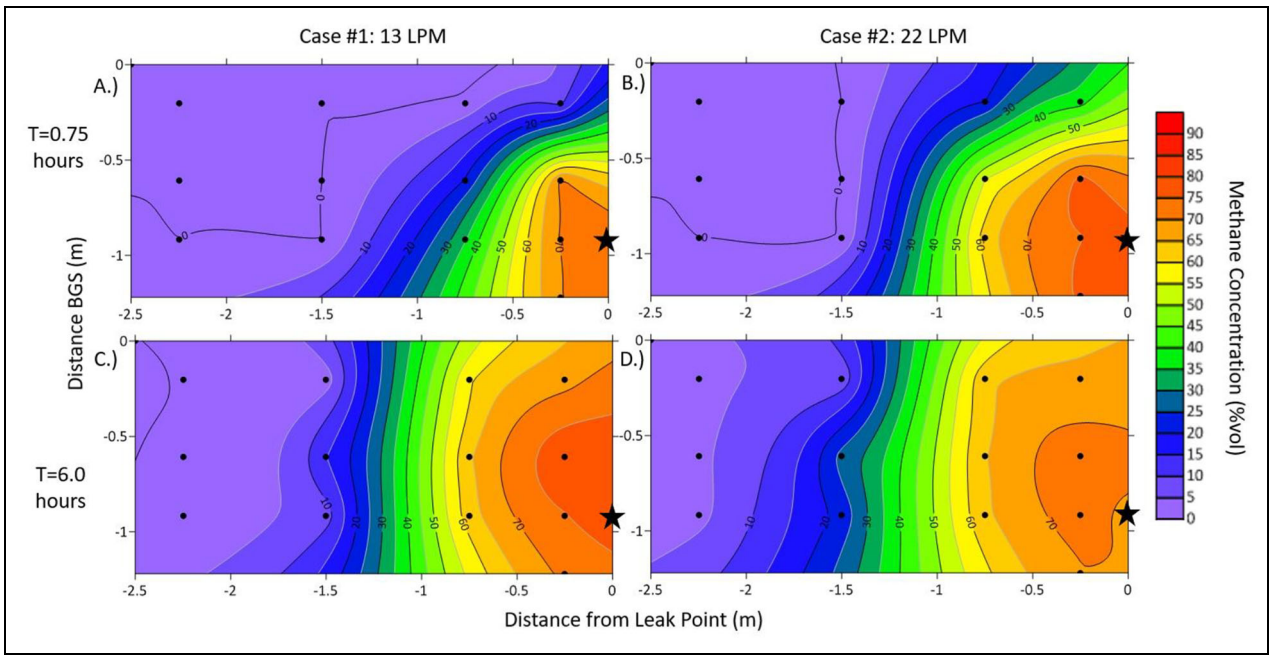

Figure 6. Observed methane concentration profiles along transect II for Cases #1 and #2 in the homogeneous bed at 0.75 and 6 h. Black stars represent the leak point location. DOI: https://doi.org/10.1525/elementa.2021.00008.f6

concentration contours, this expansion can be captured by the experimental measurements. This is because the impact of advection, which is the dominant transport mechanism near the leak point, gradually decreases to steady state as seen in **Figure 5a**, while diffusion continues to transport gas from the high concentration near the leak point toward lower concentrations in the far field (see **Figure 5b**). The effect of diffusion, which is decided by the molecular concentration gradient, is weaker than advection which is controlled by the pressure gradient.

3.2. Effect of leak rate

To investigate the effect of leakage rate on methane migration, the results of test Cases #1 (0.5 kg/h) and #2 (0.85 kg/h) were compared. The measured methane concentration distribution of these two cases at 0.75 and 6 h (**Figure 6**) show that a higher leakage rate results in faster, and initially further, migration, especially for the higher concentration contours near the leak point (see **Figure 6A** and **B**). As explained in Section 3.1, the higher concentration profiles near the leak location at initial time periods is determined by the dominant role of advection in the vicinity of the leakage. **Figure 7a** further highlights this point, comparing the simulated horizontal component of the advective fluxes under the two experimental leak rates at the early time ($t = 0.75$ h). An increasing leak rate enhances the pressure gradient surrounding the leak point and thus highlights the advection effect. As a result, the high concentration contours close to the leak point move farther under a higher leak rate. In turn, this influences the migration of the moderate to the low concentration contours, such as those of 5%vol–50%vol. Thus,

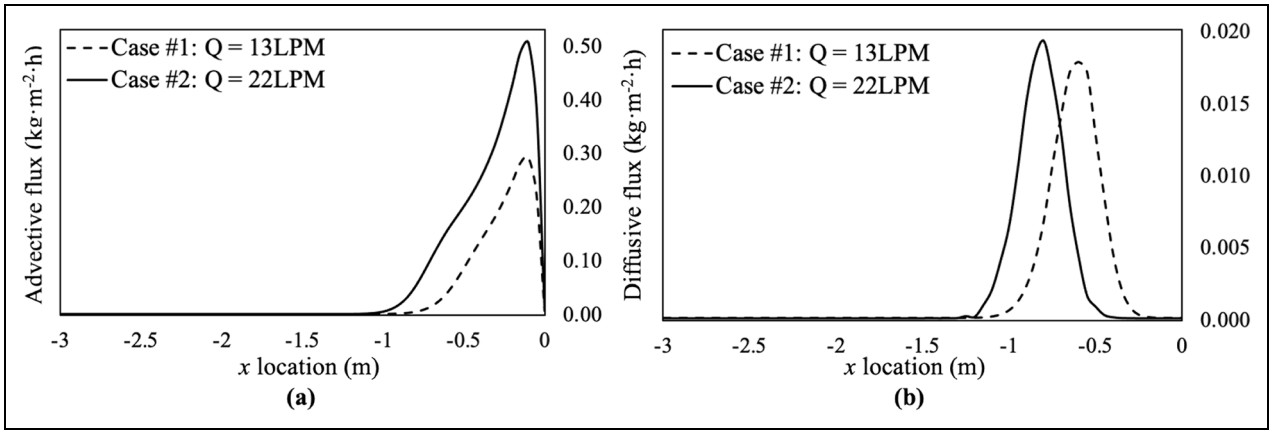

Figure 7. Simulated horizontal component of (a) advective flux and (b) diffusive flux under different leak rates at 0.7 h along a transect located 0.8 m below ground surface. Note difference in vertical axis scale. DOI: https://doi.org/10.1525/elementa.2021.00008.f7

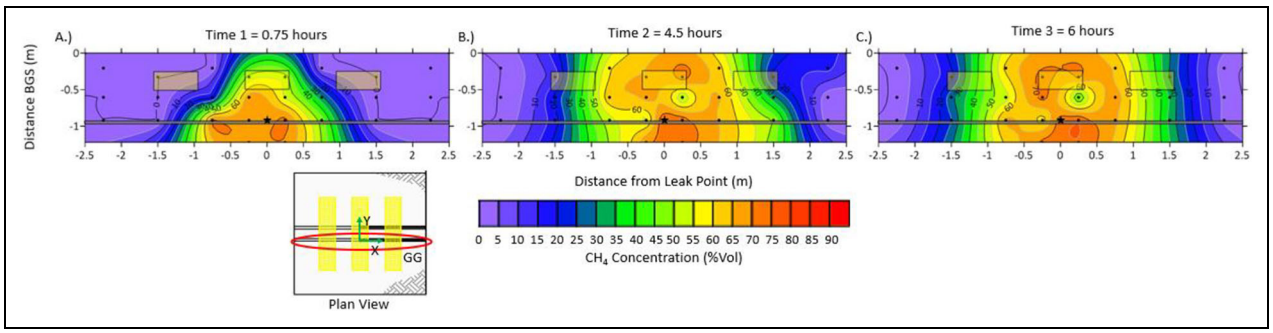

Figure 8. Observed methane concentration in the layered test bed (Case #3) at three select times along transect GG. The outlined boxes within each figure represent the location of the clay layers. The pipeline is depicted as a gray bar and the leak point as the black star. DOI: https://doi.org/10.1525/elementa.2021.00008.f8

increasing leak rate expands the influences of the diffusion effect farther away from the leakage as seen in **Figure 7b**. However, as mentioned in Section 3.1, with the gradual transition to steady state between 4.5 and 6 h after initial gas release, the high concentration contours close to the leak point change only negligibly, resulting in little outward movement of the high concentration area, while diffusion continues to move methane outward for an extended period. However, because diffusion is an order of magnitude smaller than the advection near the leak point (see **Figure 7a** and **b**), the leak rate has relatively little influence on the methane migration at later times when the leak is in steady state (see **Figure 6C** and **D**). In other words, the leak rate is important during the transient stage of methane migration, but once steady state is achieved, it has little influence on methane migration.

The analysis in this section implies three main points for leak detection and classification operations. First, gas transport behavior is different for non-steady verses steady-state conditions and therefore must be considered in operator analysis of the leakage scenario. Under non-steady-state conditions, the advective transport for high leak rates results in faster, and initially further gas migration, especially for the higher concentration contours. Diffusion impacts the spreading farther from the leak but has little influence compared to the influence of advection under non-steady-state conditions. However, over time when steady or quasi-steady-state conditions are reached, smaller and larger leak rates may result in similar areas of methane influence due to the contributions of diffusion farther from the leak source. Diffusion keeps driving methane farther away from the leak point, weakly and slowly, regardless of the leak rate. Therefore, as the leak continues over time, the area of influence slowly continues to spread. This implies that the locations commonly considered unsafe for high leak rate scenarios should also be considered for unresolved low leak scenarios. Second, for unresolved leaks, rather than only focusing routine detection efforts close the leak point, surveyors should also monitor any changes in concentration away from the leak point. Only looking at belowground gas concentration, readings adjacent and above the leak at one snapshot in time could result in the misclassification of the leak. Third, the detection and repair of a leak does not necessarily stop the previously released methane from continuing to spreading and should therefore be carefully considered in risk assessment. To improve industry best practices, we recommend that known leak locations be revisited at the outer boundaries of the leak area of

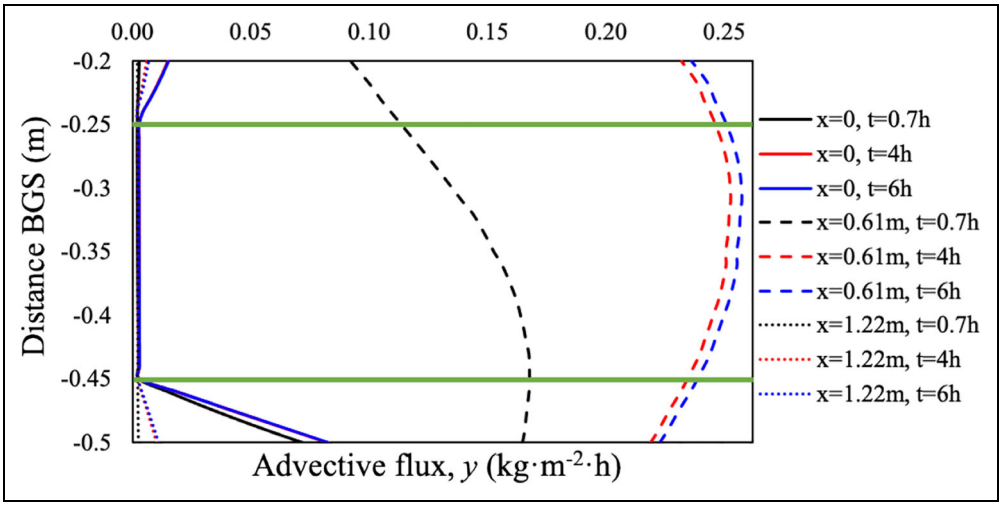

Figure 9. Simulated profiles of the vertical component of advective flux at different locations ($x = 0$, 0.61, and 1.22 m) and different times ($t = 0.7$, 4, and 6 h). $x = 0$ denotes the horizontal coordinate of the vertical centerline of the middle clay layer, also the vertical line through the leak point; $x = 0.61$ and 1.22 m denote the vertical lines in the middle between two clay layers and the middle of the rightmost clay layer, respectively. The area between two green lines is the vertical area where the three clay layers are located. DOI: https://doi.org/10.1525/elementa.2021.00008.f9

influence and to avoid any assumptions in leak spreading based on leak size estimates.

3.3. Effect of textural configuration

The effect of soil textural heterogeneity was considered in this experimental study through Case #3. The presence of the high-saturation clay layers within the soil leads to different gas migration behavior compared to the homogenous soil conditions in Cases #1 and #2. **Figure 8** depicts the measured concentration profiles at 0.75, 4.5, and 6 h for the layered soil configuration. High concentrations of methane can be seen under and adjacent to the clay layers at early times. Methane distribution, especially surrounding the leak point, changes negligibly at later times. As previously explained in Section 3.1, these behaviors are formed because advection dominates close to the leak point, especially at the early transient stage.

Since the permeability of the clay is over three orders of magnitude smaller than sand (see **Table 2**), gas preferentially migrates around the clay layers. As a result, the advection effect is more intensive in the sand than the clay layers. **Figure 9** shows the modeled profiles of the vertical component of advective flux at three locations ($x = 0$, 0.61, and 1.22 m), representing the middle of the second clay layer, between the second and third clay layers (i.e., sand area), and the middle of the third clay layer, respectively. Simulations demonstrate that advection has a significantly stronger influence on the sand area between two clay layers (dashed lines in **Figure 9**) compared to within the clay layer itself (solid and dotted lines). As time progresses, advection driven fluxes stabilize and little difference in methane distribution is observed in experiments from 4.5 to 6 h.

According to the above understanding, methane migration inside the clay layers should be slower than the surrounding sandy soil, especially during the transient stage

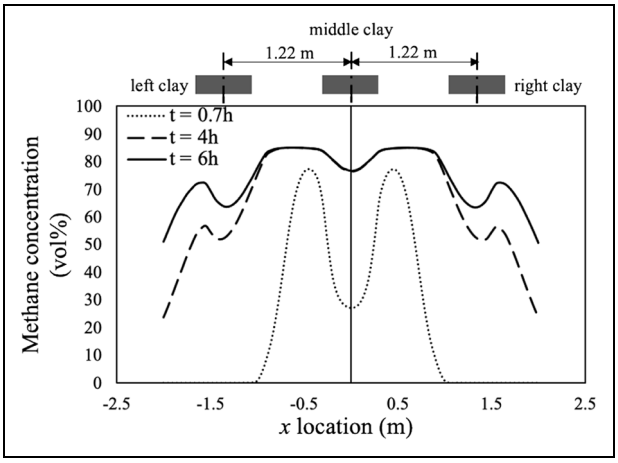

Figure 10. Simulated methane concentration distribution along the horizontal transect through the middle of the clay layers (0.25 m BGS). $x = -1.22$, 0, and 1.22 m denotes the center points of the three clay layers. The top three dark gray rectangles represent the horizontal location of the three clay layers. DOI: https://doi.org/10.1525/elementa.2021.00008.f10

early in the experiment. However, the concentration plot shown in **Figure 8A** illustrates that methane seems to break through the middle clay layer first and then moves to the two sides. This is a result of the limited concentration readings within the test bed. The vapor implants were unfortunately not located in the proper positions to capture the transient behavior. Therefore, the migration trend of methane was not well delineated. This problem also demonstrates the importance of modeling as a necessary auxiliary step when designing field experiments. **Figure 10** shows the modeled methane concentration distribution along the horizontal line 0.25 m BGS. $x = 0$ denotes

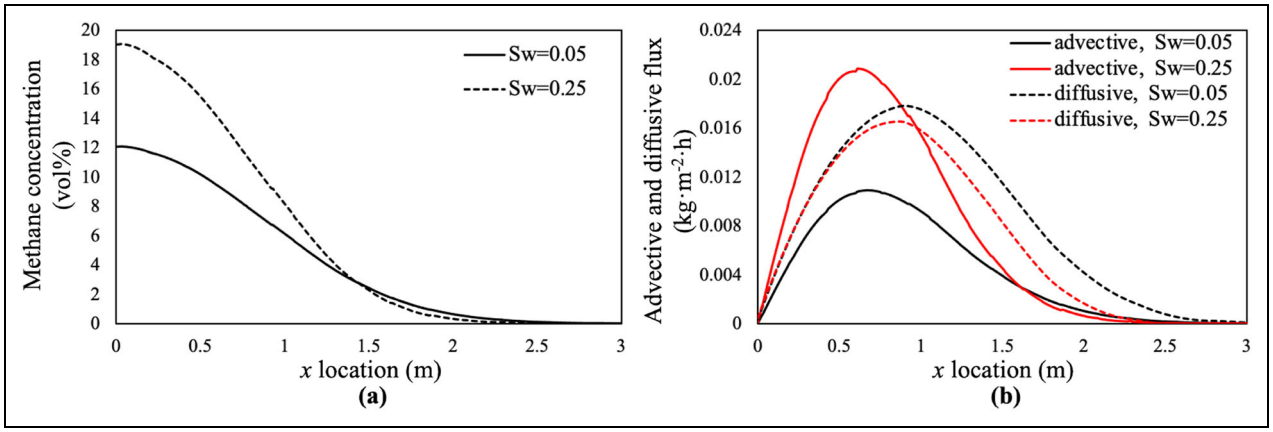

Figure 11. (a) Simulated methane concentration and (b) horizontal component value of advective and diffusive flux along a line 2 m below the computation domain surface at $t = 6$ h for different average water saturation ($S_w = 0.05$ and 0.25) setup. DOI: https://doi.org/10.1525/elementa.2021.00008.f11

the center point of the middle clay layer, where a lower concentration is seen compared to the two sides of the middle clay layer. However, the two vapor implants inside this clay layer were placed at the two sides of the layers (the black points in **Figure 8A**) rather than the middle of the layer, which recorded relatively high concentrations affected by the adjacent sandy soil. Using the limited data, the low concentrations between the two vapor implants were not captured. This disparity indicates that gas sampling locations within soil layers should be at higher spatial resolutions than for homogenous soil conditions due to the variability of concentrations within the layers as a result of the surround soil conditions. Moreover, **Figure 10** also illustrates that locally higher methane concentrations (e.g., hot spots) may be detected adjacent to a low permeable soil layer. Hot spots may continue even after a leak is repaired due to the accumulated gas underneath the low permeable soil layer. This indicates the importance of understanding the soil layering conditions during leak survey and how that layering can lead to subsurface gas distributions and transport.

3.4. Effect of soil moisture

Experimental investigation of the impact of soil moisture on subsurface methane migration was not performed due to the difficulty in creating stable and homogeneous soil saturation distributions for a field study. Instead, numerical approaches were used in this section to provide preliminary understanding. The corresponding experiments will be considered and well-designed as the next step to validate and deepen this understanding. Two average saturations of the shallow subsurface ($S_w = 0.05$ and 0.25) are considered here to compare their influence on methane movement. **Figure 11a** compares the methane concentration along a horizontal line located 2 m below the soil domain at $t = 6$ h.

In general, **Figure 11a** shows that a higher soil water saturation leads to a higher methane concentration, especially close to the leak point (e.g., 0–1.5 m). On the contrary, moving away from the leak point, the higher soil water saturation leads to a lower methane concentration. This phenomenon can be understood from two aspects.

First, water saturation has a reverse influence on the contribution of advection and diffusion to methane distribution. As illustrated by **Figure 11b**, higher soil water saturation leads to a stronger advective flux but a weaker diffusive flux. The higher soil water saturation increases the tortuosity for gas flow, thus increasing the advection while at the same time lowering the lateral diffusion. A direct result is methane accumulation and therefore high concentrations near the leak point. Second, the relative contribution of advection and diffusion to methane distribution varies with distance from the leak point. **Figure 11b** shows that even when a soil has a higher water saturation, moving away from the leak point (e.g., x is about 1.5 m), the advective flux will become smaller than for a lower saturated soil at the same distance. However, the diffusive flux always remains larger for a soil with a lower saturation. Thus, at the locations that are far away from leak sources, a higher methane concentration will be observed for a lower saturated soil.

Figure 11a also provides insight into the relative change in concentration with distance from the leak location for high and low saturated soils. Compared to the high saturation condition, for a relatively dry soil, the methane concentration decreases gradually with distance from the leak point. In practice, this behavior indicates the need to understand the methane concentration relative to the soil moisture. If readings are taken under saturated soil conditions when the gas transport is impeded, this could result in the misclassification of a leak, especially the area of influence with soil drying. The surveyor should therefore record the moisture conditions of the soil to determine whether the leak would be expected to be more widely spread or more concentrated at the leak point. To improve industry best practice, this also indicates the need to monitor methane concentrations far from the leak source and any change in gas spreading over time. This is especially important in scenarios where the soil moisture conditions may vary due to rainfall or

a belowground or adjacent water source that can quickly change the soil moisture conditions and impact methane migration behavior.

4. Conclusions

Using a field-scale test facility linked with numerical modeling, this study investigated the effects of soil moisture, texture, and leakage rate on NG transport from below ground pipeline leaks. Results show that for a homogeneous soil system, concentric subsurface methane concentration contours centered on the leak point are found both parallel and perpendicular to the pipeline. The concentration contours approaching the leak point are sparsely distributed but become denser when stepping away from the leak point until the concentration decreases to an infinitesimal value.

The scenarios presented here highlight the importance of understanding the relative effects of advection and diffusion on methane transport. Under transient conditions, the migration behavior is dominated by the contribution of advective transport, which plays a dominant role near the leak source due to the pressure gradient caused by gas release. As the impact of advection approaches steady state, the high concentration contours show negligible outward movement, while low concentration contours farther from the leak point are observed moving outward principally driven by diffusion caused by the molecular concentration gradient. Because of this mechanism, the leak rate within the range of conditions tested has little effect on the spreading width of the methane plume when approaching steady state but shows more outstretched high-concentration contours at higher leak rates under transient conditions.

The differences in the dominant impact of advection and diffusion relative to the leak point suggest that known leaks that are not immediately repaired should be regularly revisited, focusing on understanding any variation in the concentrations and distances the gas has traveled. Even if the leak source can be repaired, the distant areas with elevated concentration should not be ignored; the originally released methane may keep moving and accumulating below ground.

Increasing soil moisture results in farther migration of high-concentration contours as the high-water saturation increases advective transport near the leak. However, this results in a relatively smaller overall methane plume since the higher saturation lowers the diffusivity which dominates transport farther from the leak. This phenomenon is especially important to understand in arid and semiarid regions that experience intermittent rainfall or variable water table conditions that may influence moisture availability. As soil dries, methane diffusion will increase, and therefore, the distance of elevated gas concentrations may increase. In addition, due to the large permeability difference for a layered soil system consisting of a clay and sand, advection effects are especially significant in the more permeable area (e.g., sand), leading to enhanced migration in the sand and slow migration inside the clay. Hence, locally high methane concentrations may be observed adjacent to the clay layers. Understanding the soil compositions in a region where pipeline leak occurs may help locate and explain the presence of elevated concentrations.

In addition to the conditions tested here, many other factors, such as investigating the effect of trenched bed systems or fractured soils, vegetation or surface obstructions, the leak orientation, and varying atmospheric conditions on gas migration, should be included in the analysis of gas leakage scenarios to improve industry best practices and understand the relative effects of conditions on gas transport behavior.

Data accessibility statement

All data sets used in this article, including methane concentration measured in the Methane Emission Technology Evaluation Center field test bed and modeling outputs, are available in these in-text data citation references: Smits (2021).

Supplemental files

The supplemental files for this article can be found as follows:

Numerical data processing.xlsx.

METEC Paper CH4 Experimental Data.xlsx.

Supplemental data for Study of Methane Migration in Shallow Subsurface from a Gas Pipe Leak.doc.

Smits, Kathleen, 2021, "Replication Data for: Study of Methane Migration in the Shallow Subsurface From a Gas Pipe Leak", https://doi.org/10.18738/T8/MOC3L9, Texas Data Repository, V1.

Acknowledgments

Any opinion, findings, and conclusions or recommendations expressed herein are those of the authors and do not necessarily reflect the views of those providing technical input or financial support. The trade names mentioned herein are merely for identification purposes and do not constitute endorsement by any entity involved in this study.

Funding

This research was funded in part by the U.S. Department of Energy's Advanced Research Projects Agency—Energy Methane Observation Networks with Innovative Technology to Obtain Reductions (ARPA-E MONITOR; #DE-FOA-0001546), the U.S. Department of Transportation Pipeline and Hazardous Materials Safety Administration (PHMSA) under Grant No. 693JK31810013, and the National Science Foundation Project Award Number 1447533.

Competing interests

The authors declared that they have no conflicts of interest to this work.

Author contributions

Devised and supervised the whole project: KMS.

Developed the theoretical models, performed the simulations, and analyzed the results: BG.

Carried out the experiment and processed the experimental data: MKM.

Provided ideas and assisted with experimental design and measurement: CB, DZ, CDTKK, AH.
Took the lead in writing the manuscript: BG, MKM.
Provided critical feedback and helped shape the research, analysis, and manuscript: All authors.

References

Annual Report Mileage for Gas Distribution Systems. 2020. Available at U.S. Department of Transportation website: https://www.phmsa.dot.gov/data-and-statistics/pipeline/annual-report-mileage-gas-distribution-systems. Accessed 25 December 2020.

Bahlmann, LM, Smits, KM, Heck, K, Coltman, E, Helmig, R, Neuweiler, I. 2020. Gas component transport across the soil-atmosphere interface for gases of different density: Experiments and modeling. *Water Resources Research* **56**(9): e2020WR027600. DOI: http://dx.doi.org/10.1029/2020WR027600.

Basirat, F, Sharma, P, Fagerlund, F, Niemi, A. 2015. Experimental and modeling investigation of CO2 flow and transport in a coupled domain of porous media and free flow. *International Journal of Greenhouse Gas Control* **42**: 461–470. DOI: http://dx.doi.org/10.1016/j.ijggc.2015.08.024.

Brutsaert, W. 1982. *Evaporation into the atmosphere, theory, history, and application. Kluwer Academic Publishers*. Dordrecht, the Netherlands: Kluwer Academic.

Camillo, PJ, Gurney, RJ. 1986. A resistance parameter for bare-soil evaporation models. *Soil Science* **141**(2): 95–105. DOI: http://dx.doi.org/10.1097/00010694-198602000-00001.

Cho, Y, Ulrich, BA, Zimmerle, DJ, Smits, KM. 2020. Estimating natural gas emissions from underground pipelines using surface concentration measurements. *Environmental Pollution* **267**: 115514. DOI: http://dx.doi.org/10.1016/j.envpol.2020.115514.

Deepagoda, TKKC, Smits, KM, Oldenburg, CM. 2016. Effect of subsurface soil moisture variability and atmospheric conditions on methane gas migration in shallow subsurface. *International Journal of Greenhouse Gas Control* **55**: 105–117. DOI: http://dx.doi.org/10.1016/j.ijggc.2016.10.016.

Electronic Code of Federal Regulations §192.327 Cover. 2021. E-CFR. Available at Western Regional Gas Conference website: https://www.ecfr.gov/cgi-bin/retrieveECFR?gp=1&SID=c3b0e911814b61c0f807c43f51ac7bc6&ty=HTML&h=L&mc=true&r=SECTION&n=se49.3.192_1327. Accessed 6 January 2021.

Foster, CS, Crosman, ET, Horel, JD, Lyman, S, Fasoli, B, Bares, R, Lin, JC, Helmig, D, Lamb, B. 2019. Quantifying methane emissions in the Uintah Basin during wintertime stagnation episodes. *Elementa: Science of the Anthropocene* **7**(1). DOI: http://dx.doi.org/10.1525/elementa.362.

Heldenbrand, D, Saavedra, D. 2019. New concepts for soil gas migration. Available at http://www.westernregionalgas.org/2019/presentations/SoilGasMigrationConceptsDHeldenbrandWRGC2019.pdf. Accessed 1 July 2021.

Hibi, Y, Fujinawa, K, Nishizaki, S, Okamura, K, Tasaki, M. 2009. Multi-component migration in the gas phase of soil: Comparison between results of experiments and simulation by dusty gas model. *Soils and Foundations* **49**(4): 569–581. DOI: http://dx.doi.org/10.3208/sandf.49.569.

Hibi, Y, Kanou, Y, Ohira, Y. 2012. Estimation of mechanical dispersion and dispersivity in a soil–gas system by column experiments and the dusty gas model. *Journal of Contaminant Hydrology* **131**(1–4): 39–53. DOI: http://dx.doi.org/10.1016/j.jconhyd.2012.01.003.

Iwata, T, Hamaide, G, Fuchimoto, K. 1992. Development of analytical methods for the behavior of underground leakage gas from low-pressure mains. *International Gas Research Conference Proceedings* **1**: 1302–1311.

Jackson, RB, Down, A, Phillips, NG, Ackley, RC, Cook, CW, Plata, DL, Zhao, K. 2014. Natural gas pipeline leaks across Washington, DC. *Environmental Science & Technology* **48**(3): 2051–2058. DOI: http://dx.doi.org/10.1021/es404474x.

Karl-Heinz, AA, Siemons, N, Bruining, J. 2004. Multiphase flow experiments in order to understand the behaviour of (partly) saturated coals as a gas reservoir: Examples. *Geologica Belgica* **7/3**(4): 115–121.

Keskikuru, T, Kokotti, H, Lammi, S, Kalliokoski, P. 2001. Effect of various factors on the rate of radon entry into two different types of houses. *Building and Environment* **36**(10): 1091–1098. DOI: http://dx.doi.org/10.1016/S0360-1323(00)00077-9.

Levintal, E, Dragila, MI, Kamai, T, Weisbrod, N. 2017. Free and forced gas advection in highly permeable, dry porous media. *Agricultural and Forest Meteorology* **232**: 469–478. DOI: http://dx.doi.org/10.1016/j.agrformet.2016.10.001.

Millington, RJ, Quirk, JP. 1961. Permeability of porous solids. *Transactions of the Faraday Society* **57**: 1200–1207. DOI: http://dx.doi.org/10.1039/TF9615701200.

Okamoto, H, Gomi, Y. 2011. Empirical research on diffusion behavior of leaked gas in the ground. *Journal of Loss Prevention in the Process Industries* **24**(5): 531–540. DOI: http://dx.doi.org/10.1016/j.jlp.2011.01.007.

Oldenburg, CM, Unger, AJA. 2004. Coupled vadose zone and atmospheric surface-layer transport of carbon dioxide from geologic carbon sequestration sites. *Vadose Zone Journal* **3**(3): 848–857. DOI: http://dx.doi.org/10.2136/vzj2004.0848.

Patterson, BM, Davis, GB. 2009. Quantification of vapor intrusion pathways into a slab-on-ground building under varying environmental conditions. *Environmental Science & Technology* **43**(3): 650–656. DOI: http://dx.doi.org/10.1021/es801334x.

Poulsen, TG, Christophersen, M, Moldrup, P, Kjeldsen, P. 2003. Relating landfill gas emissions to atmospheric pressure using numerical modelling and

state-space analysis. *Waste Management & Research* **21**(4): 356–366. DOI: http://dx.doi.org/10.1177/0734242x0302100408.

Poulsen, TG, Furman, A, Liberzon, D. 2017. Effects of wind speed and wind gustiness on subsurface gas transport. *Vadose Zone Journal* **16**(11): 1–10. DOI: http://dx.doi.org/10.2136/vzj2017.04.0079.

Poulsen, TG, Furman, A, Liberzon, D. 2018. Effect of near-surface wind speed and gustiness on horizontal and vertical porous medium gas transport and gas exchange with the atmosphere. *European Journal of Soil Science* **69**(2): 279–289. DOI: http://dx.doi.org/10.1111/ejss.12531.

Pourbakhtiar, A, Poulsen, TG, Wilkinson, S, Bridge, JW. 2017. Effect of wind turbulence on gas transport in porous media: Experimental method and preliminary results. *European Journal of Soil Science* **68**(1): 48–56. DOI: http://dx.doi.org/10.1111/ejss.12403.

Ravikumar, AP, Sreedhara, S, Wang, J, Englander, J, Roda-Stuart, D, Bell, C, Zimmerle, D, Lyon, D, Mogstad, I, Ratner, B, Brandt, AR. 2019. Single-blind inter-comparison of methane detection technologies–results from the Stanford/EDF Mobile Monitoring Challenge. *Elementa: Science of the Anthropocene* **7**. DOI: http://dx.doi.org/10.1525/elementa.373.

Smits, K. 2021. Replication data for: Study of methane migration in the shallow subsurface from a gas pipe leak. *Texas Data Repository* **V1**. DOI: http://dx.doi.org/10.18738/T8/MOC3L9.

Taherdangkoo, R, Tatomir, A, Sauter, M. 2020. Modeling of methane migration from gas wellbores into shallow groundwater at basin scale. *Environmental Earth Sciences* **79**(18): 1–16. DOI: http://dx.doi.org/10.1007/s12665-020-09170-5.

Ulrich, BA, Mitton, M, Lachenmeyer, E, Hecobian, A, Zimmerle, D, Smits, KM. 2019. Natural gas emissions from underground pipelines and implications for leak detection. *Environmental Science & Technology Letters* **6**(7): 401–406. DOI: http://dx.doi.org/10.1021/acs.estlett.9b00291.

U.S. Department of Transportation Pipeline and Hazardous Material Safety Administration. 2020. Incident statistics. Available at https://www.phmsa.dot.gov/hazmat-program-management-data-and-statistics/data-operations/incident-statistics. Accessed 1 June 2021.

Vanderborght, J, Fetzer, T, Mosthaf, K, Smits, KM, Helmig, R. 2017. Heat and water transport in soils and across the soil-atmosphere interface: 1. Theory and different model concepts. *Water Resources Research* **53**(2): 1057–1079. DOI: http://dx.doi.org/10.1002/2016WR019982.

Van De Ven, CJ, Abraham, JE, Mumford, KG. 2020. Laboratory investigation of free-phase stray gas migration in shallow aquifers using modified light transmission. *Advances in Water Resources* **139**. DOI: http://dx.doi.org/10.1016/j.advwatres.2020.103543.

Van Genuchten, MT. 1980. A closed-form equation for predicting the hydraulic conductivity of unsaturated soils. *Soil Science Society of America Journal* **44**(5): 892–898. DOI: http://dx.doi.org/10.2136/sssaj1980.03615995004400050002x.

von Fischer, JC, Cooley, D, Chamberlain, S, Gaylord, A, Griebenow, CJ, Hamburg, SP, Salo, J, Schumacher, R, Theobald, D, Ham, J. 2017. Rapid, vehicle-based identification of location and magnitude of urban natural gas pipeline leaks. *Environmental Science & Technology* **51**(7): 4091–4099. DOI: http://dx.doi.org/10.1021/acs.est.6b06095.

Wang, G, Ma, S, Ström, J, Suuberg, E, Yao, Y, Zeng, L. 2019. Investigating two-dimensional soil gas transport of trichloroethylene in vapor intrusion scenarios involving surface pavements using a pilot-scale tank. *Journal of Hazardous Materials* **371**: 138–145. DOI: http://dx.doi.org/10.1016/j.jhazmat.2019.02.069.

Wang, G, Xiao, Y, Zuo, J, Wang, Y, Man, J, Tang, W, Chen, Q, Ma, S, Yao, Y. 2020. Physically simulating the effect of lateral vapor source-building separation on soil vapor intrusion: Influences of surface pavements and soil heterogeneity. *Journal of Contaminant Hydrology*, **235**. DOI: http://dx.doi.org/10.1016/j.jconhyd.2020.103712.

Wieringa, J. 1980. Representativeness of wind observations at airports. *Bulletin of the American Meteorological Society* **61**(9): 962–971. DOI: http://dx.doi.org/10.1175/1520-0477(1980)061<0962:ROWOAA<2.0.CO;2.

Xie, Y, Wang, T, Lü, L, Bai, Y, Song, B, Zhang, X. 2015. Full-scale experiment of diffusion behaviors of city pipeline gas in soils. *Natural Gas Industry* **35**(8): 106–113. DOI: http://dx.doi.org/10.3787/j.issn.1000-0976.2015.08.016.

Yan, Y, Dong, X, Li, J. 2015. Experimental study of methane diffusion in soil for an underground gas pipe leak. *Journal of Natural Gas Science and Engineering* **27**: 82–89. DOI: http://dx.doi.org/10.1016/j.jngse.2015.08.039.

Yao, Y, Wang, Y, Zhong, Z, Tang, M, Suuberg, EM. 2017. Investigating the role of soil texture in vapor intrusion from groundwater sources. *Journal of Environmental Quality* **46**(4): 776–784. DOI: http://dx.doi.org/10.2134/jeq2017.01.0011.

How to cite this article: Gao, B, Mitton, MK, Bell, C, Zimmerle, D, Chamindu Deepagoda, TKK, Hecobian, A, Smits, KM. 2021. Study of methane migration in the shallow subsurface from a gas pipe leak. *Elementa: Science of the Anthropocene* 9(1). DOI: https://doi.org/10.1525/elementa.2021.00008

Domain Editor-in-Chief: Steven Allison, University of California, Irvine, CA, USA

Associate Editor: Peter M. Homyak, University of California, Riverside, CA, USA

Knowledge Domain: Ecology and Earth Systems

Published: July 2, 2021 **Accepted:** June 4, 2021 **Submitted:** February 2, 2021

ELEMENTA Science of the Anthropocene

Elem Sci Anth is a peer-reviewed open access journal published by University of California Press.

OPEN ACCESS